

---

# Larch (*Larix sibirica* Ledeb.) and Poplar (*Populus laurifolia* Ledeb.) Are Moving into the Goby Desert

---

[Viacheslav I. Kharuk](#)<sup>\*</sup>, [Il'ya A. Petrov](#), [Sergei T. Im](#), Alexander S. Shushpanov, Sergei O. Ondar, [Andrey M. Samdan](#)

Posted Date: 3 February 2026

doi: 10.20944/preprints202602.0151.v1

Keywords: larch southward migration; poplar southward migration; larch refugia; forest-non-forest ecotone; trees in desert; larch range in Siberia; poplar range in Siberia; southward trees migration



Preprints.org is a free multidisciplinary platform providing preprint service that is dedicated to making early versions of research outputs permanently available and citable. Preprints posted at Preprints.org appear in Web of Science, Crossref, Google Scholar, Scilit, Europe PMC.

Copyright: This open access article is published under a [Creative Commons CC BY 4.0 license](#), which permit the free download, distribution, and reuse, provided that the author and preprint are cited in any reuse.

Disclaimer/Publisher's Note: The statements, opinions, and data contained in all publications are solely those of the individual author(s) and contributor(s) and not of MDPI and/or the editor(s). MDPI and/or the editor(s) disclaim responsibility for any injury to people or property resulting from any ideas, methods, instructions, or products referred to in the content.

Article

# Larch (*Larix sibirica* Ledeb.) and Poplar (*Populus laurifolia* Ledeb.) Are Moving into the Goby Desert

Viacheslav I. Kharuk <sup>1,2,\*</sup>, Il'ya A. Petrov <sup>1,2</sup>, Sergei T. Im <sup>1,2,3</sup>, Alexander S. Shushpanov <sup>1,3</sup>, Sergei O. Ondar <sup>4</sup> and Andrey M. Samdan <sup>4</sup>

<sup>1</sup> Sukachev Institute of Forests, Federal Scientific Center, Russian Academy of Science, Siberian Branch, Academgorodok 50/28, Krasnoyarsk 660036, Russia

<sup>2</sup> Institute of Space and Information Technologies, Institute of Ecology and Geography, Siberian Federal University, Svobodny Str. 79, Krasnoyarsk 660041, Russia

<sup>3</sup> Institute of Space Research and High Technologies, Reshetnev Siberian State University of Science and Technology, Krasnoyarsky Rabochy Str. 31, Krasnoyarsk 660014, Russia

<sup>4</sup> Department of Biology and Ecology, Tuvan State University, Lenina Str. 36, Kyzyl 667000, Russia

\* Correspondence: v7sib@mail.ru

## Abstract

Trees in the ecotones are most sensitive to the changing climate. Here we analyzed growth and dynamics of larch and poplar trees in the unique refugia that border Mongolian desert in southern Siberia. We aimed to analyze (1) larch (*Larix sibirica* Ledeb.) and poplar (*Populus laurifolia* Ledeb.) radial growth dependence on climate variables, (2) tree migration into desert, and (3) gross primary production (GPP) of ground cover in refugia and in the adjacent desert. We used on-ground survey, dendroecological methods, and remote sensing analysis (satellite and Unmanned Aerial Vehicle, UAV). We found that the larch population in refugia consists of an old-growth cohort and a young cohort. The age of old-growth trees ( $A = 500+$ ) indicates that refugia may have existed throughout the Holocene. The young cohort ( $A = 50+$ ) has existed since the warming onset in the 1970th. The poplar population includes single old-growth specimens ( $A > 200$  y) and young trees ( $A = 50+$  y). Growth of both larch and poplar species is controlled by air and soil droughts (indicated by SPEI and scPDSI indexes, respectively). Old-growth larch trees are less sensitive to available moisture compared with young larch and poplar. Summer winds impair larch growth. In the 21st century, populations increased by +46% and +36% (for larch and poplar, respectively). Both larch and poplar trees are slowly migrating into the adjacent desert. Unexpectedly, poplar trees spread ahead of the more drought-resistant larch into the desert (by 280 m vs 35 m for larch). Poplar, due to its higher seed production, is pioneer tree species that occupies new niches caused by the changing hydrology regime. We found that desert vegetation, which is composed of small bushes, is "greening" due to GPP increase. The increased population and growth of larch and poplar trees, together with their migration into the desert, contradict the predicted shrinkage of their range at its southern boundary. However, the predicted increase of moisture deficit may impair the acceleration of tree growth and its southward migration in the future. Nevertheless, current changes in climate are favorable for the growth of trees and shrubs at the northern boundary of the Great Gobi Desert.

**Keywords:** larch southward migration; poplar southward migration; larch refugia; forest-non-forest ecotone; trees in desert; larch range in Siberia; poplar range in Siberia; southward trees migration

## 1. Introduction

Larch (*Larix* spp.) is the dominant conifer species in Siberia. Larch-dominant communities (*Larix sibirica* Ledeb., *L. gmelinii* Rupr. and *L. cajanderi* Mayr.) are the largest forest formation in Russia, which cover more than 40% of the forested area. The majority of the larch-dominant forests (>95%)

are located in Siberia and cover about 70% of the permafrost zone. In severe climatic habitats, they form pure stands.

Due to its high cold-resistance, larch forms treelines in the northern and alpine forest-tundra ecotones. Larch is highly drought-resistant due to its high efficiency of water use [1]. This allows larch to grow at the semi-desert level of precipitation and to populate forest-steppe ecotones. A deep and well-developed root system allows larch to grow on drained soils with poor water and minerals content. However, within permafrost zone, the root system of larch is shallow (up to 30 cm or less).

Larches are anemochoric species with a life span up to 600–700 yrs. (up to more than 1,000 yrs in the north of Eastern Siberia). Larches are the most photophilous, shade-intolerant, and fast-growing conifer species. These species are also well adapted to wildfires and populate post-fire burns with abundant seedlings [2]. In a warmer and drier climate, larch has been considered a potential substitute for precipitation-sensitive *Abies sibirica* Ledeb., *Pinus sibirica* Du Tour, and *Picea obovata* Ledeb.) in southern lowlands of Siberia [3]. Observed climate changes are mostly favorable for larch species within the majority of their range. Thus, since the warming start in the 1970-s, *L. sibirica* tree growth in general has increased and larch-dominant forest densification is being observed in the Ural and Siberian Mountains [4–6]. Larch trees are moving uphill in mountains and northward in the polar tundra [7,8].

However, in the changing hydrothermal regime larch may experience limitation by moisture, followed by growth decrease, which has been documented within larch southern lowland habitats and at high latitudes [5,7,9,10]. Prognostic models suggest that changes in tree ranges and growth will primarily occur between the forest and non-forest ecotones [11]. Thus, larch-dominant forests within forest-steppe ecotone (the Trans-Baikal zone) have experienced thinning and mortality due to increased fire rate [2]. Globally, according to Mamet et al. [12], *Larix* has experienced northern expansion and southern retraction as species respond to changing climate.

Meanwhile, there are still only a handful of data about the larch growth and vitality at the southern range of its habitat in the changing hydrothermal regime. In this paper, we aimed to analyze the unique larch forest that is growing at the very edge of larch range on the sandy dunes at the Mongolian border, at the northern boundary part of the Gobi Desert. In fact, that site (we called it “Tes-Hem”) is a larch refugium. Together with larch, *Populus laurifolia* is also present in that area, although that species is less drought-resistant than larch. *P. laurifolia* is a typical species in Siberia and is often found within river valleys and, more rarely, in the forest-steppe ecotone.

Tested hypothesis: the changing hydrological regime may stimulate growth of *Larix sibirica* and *Populus laurifolia* and facilitate their migration into sandy dunes.

We are seeking the answers to the following questions:

1. What is long-term larch growth dynamics in the larch refugium?
2. What is the age structure of the larch trees?
3. What are migration rates of the larch and poplar into sandy dunes?
4. What are the GPP dynamics of the vegetation in that site?
5. What is the relationship between tree growth and migration, GPP, on one side, and eco-climate variables and relief features on the other?

## 2. Materials and Methods

The studies were based on field survey data, Terra/MODIS and high-res satellite time series, UAV data, trees growth index (GI) data, and regression analysis between GI and eco-climate variables. Alongside, we modeled the moisture deficit at the end of this century (2080-2100).

### 2.1. Study Area

Study sites were located on the northern boundary of the Gobi Desert. Sites included two larch refugia, i.e., “Tes-Hem” (the main site) and “Kara-Haya” (supplementary site) (Figure 1).

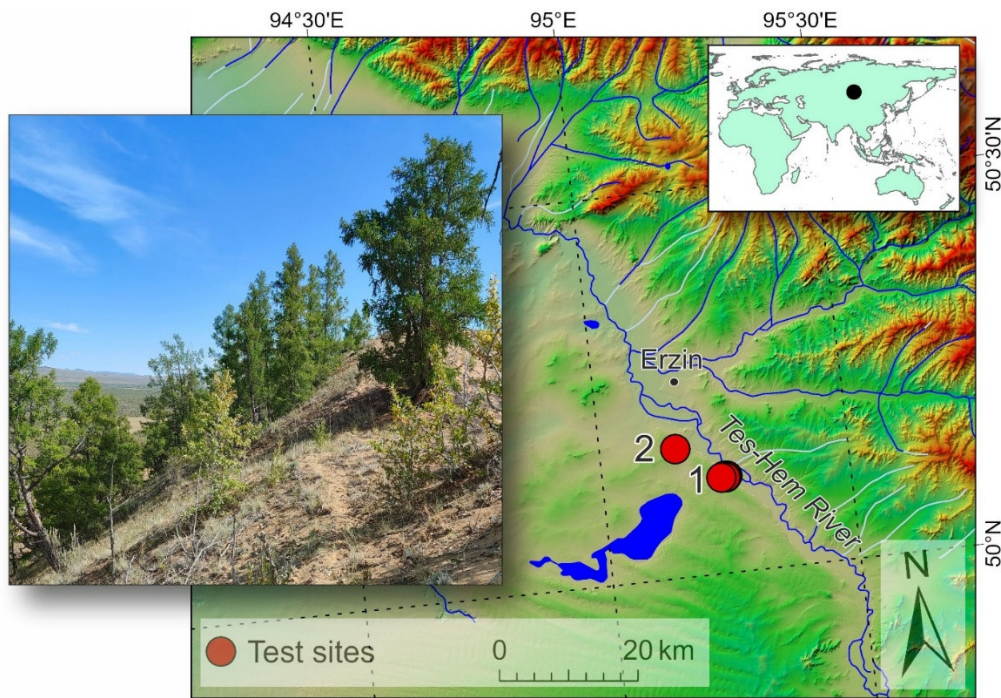


**Figure 1.** Test sites' location: 1- "Tes-Hem", 2 - "Kara-Haya".

Trees both poplar (mean height ~2 m up to 4 m and mean diameter 6.5 cm) and larch (mean height ~13 m up to 18 m and mean diameter 35-38 cm) formed clusters with closure ~0.4 as well as a separate single trees. Old-growth larches also presented in the multi-stem forms. The mean crown closure was about 0.1. Both species are growing on poor organic sandy soils (Figure 2).

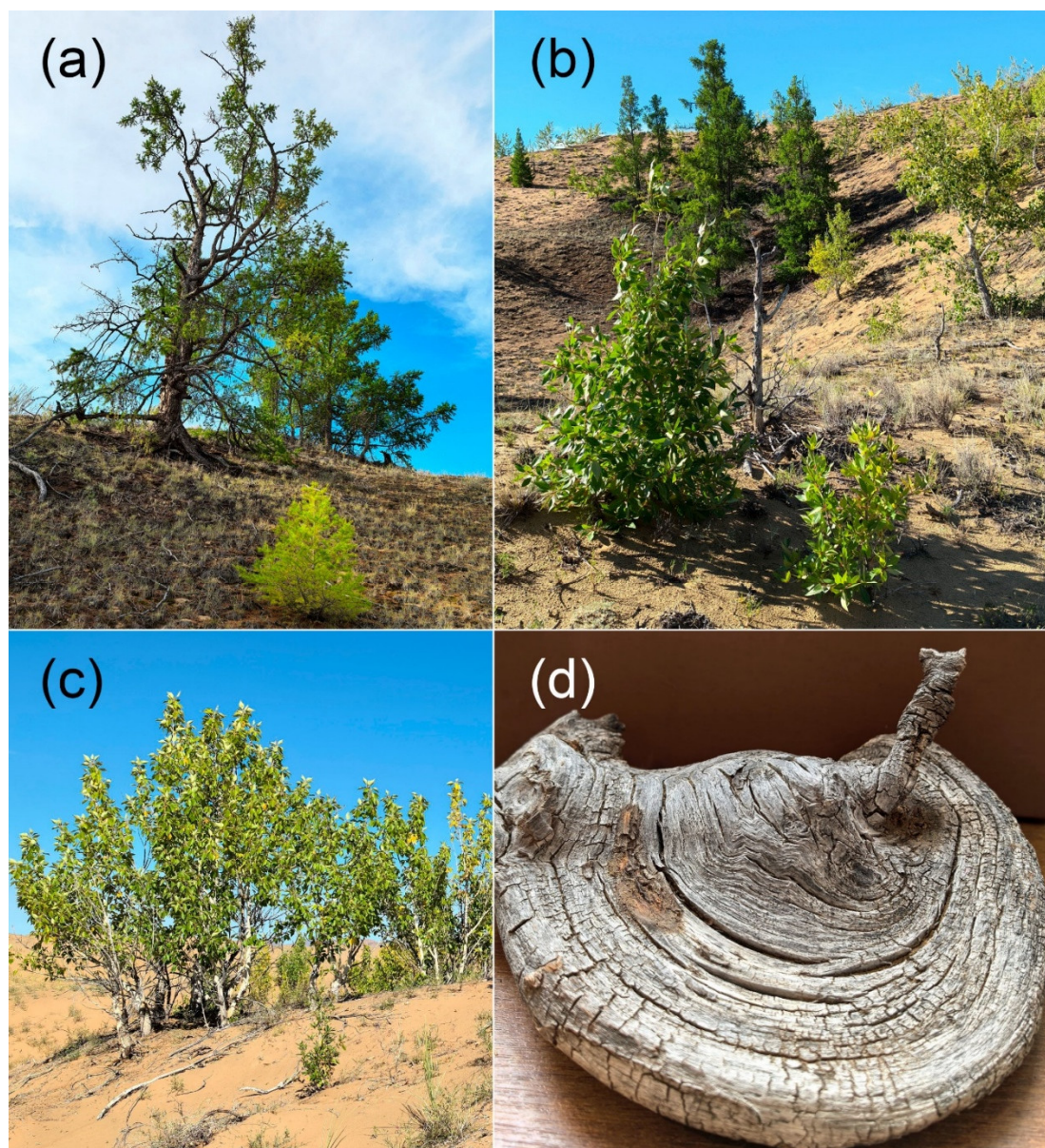


**Figure 2.** (a), (b) old-growth larch and poplar trees and regeneration. (c) Mature poplar and regeneration. (d) A specimen of fossil old-growth polar tree with estimated age > 200 y.

On-ground vegetation formed by shrubs and some grasses with ground cover about ~10-15%. It composed by *Berberis sibirica* Pall., *Cotoneaster melanocarpus* Fisch., *Caragana bungei* Ledeb., *Artemisia* spp., *Agropyron* spp., *Oxytropis tragacanthoides* Fisch., *Hedysarum fruticosum* Pall., *Thesium tuvinense* Krasnob.. Rare small moss communities (*Rhytidium rugosum* (Hedw.) Kindb. + *Polytrichum* sp.) located in the larches shadow.

## 2.2. Ground Survey Data

Fieldworks were conducted in 2025 y. Temporary test sites (N = 12) with radius of 9.8 m (S ~0.03 ha) were established within the elevation range 1100–1240 m a.s.l. We describe relief features (elevation a.s.l., aspect and slope steepness). We obtained geobotanical and soil type data. We measured tree height and DBH (diameter at breast height, 1.3 m), described tree physiognomy and stand closure, regeneration density and vitality. For dendrochronological analysis, trees were randomly selected around the area of approximately 1.0 ha. Samples (cores) were taken at DBH height or at the root collar level with an increment borer. In total, 77 larch and 17 poplar trees were sampled.

### 2.3. Eco-Climate Variables

Eco-climate variables were obtained from the ERA5-Land database and from the nearest weather station Erzin (WMO index #36307, 50°16'N, 95°10'E, H = 1102 m, distance to test sites is 10 - 20 km) using the AISORI online database [13]. Air and soil droughts were estimated based on the SPEI (Standardized Precipitation Evapotranspiration Index) index [14] and Palmer's scPDSI (Self-Calibrated Palmer Drought Severity Index) [15] and soil moisture content.

The SPEI is a proxy for atmospheric drought [16]. The increase in the SPEI indicates a decrease in atmospheric drought, and vice versa. The SPEI was calculated based on precipitation and evaporation data extracted from the ERA5-Land database using the SPEI library (v.1.8.1) [16,17] with scripting in RStudio v.2025.09.1 build 375 [18].

The scPDSI was calculated in R-Studio using the R v.4.5.1 programming language [19] and scPDSI library (v0.1.3) [20]. The input parameters were total monthly precipitation and potential evapotranspiration which were extracted from the ERA5-Land database [21]. Negative values of scPDSI indicate drought conditions, and positive ones indicate wet conditions [15].

We estimated the total water content below ground by using equivalent water thickness anomalies (EWTA) obtained from GRACE (Gravity Recovery And Climate Experiment). The monthly EWTA data were downloaded using NASA GRACE(-FO) Data Analysis Tool [22] for the period of 2002–2024 with the spatial resolution of one degree. EWTA is a measure that quantifies changes in the total amount of water stored on land, including soil moisture, snow, and groundwater relative to the 2004–2009 time-mean baseline [23]. These gravimetric data represent the vertical thickness of a layer of water that would result from the measured change in terrestrial water mass [24]. The EWTA provides a valuable tool for monitoring drought [25,26], the water cycle [27] and its impact on vegetation [28–30]. Hereafter, we shall use the term “total water content” (TWC) instead of EWTA.

### 2.4. Moisture Deficit Prognosis

As a proxy of the moisture deficit, we used the annual difference ( $\Delta$ ) between the total annual precipitation (PRE) and evaporation (E). We applied monthly climate data extracted from CMIP6, based on the CNRM-CM6-1-HR model [31] with a spatial resolution of  $\sim 0.5^\circ \times 0.5^\circ$  to estimate PRE and E. This model was chosen because its values are close to the average of all models presented in the IPCC WGI Interactive Atlas tool [32]. We analyzed data corresponding to climatic scenarios SSP4.5, SSP7.0 and SSP8.5 [33,34]. We fitted the forecast data (PRE and E) to the historical data extracted from the ERA5-Land database using the simple shift method, i.e., the forecasted monthly values were shifted by an amount equal to the average difference between the forecast and actual data for 2015–2024 (the overlap period between the forecast and historical data). We calculated and compared  $\Delta$  between 2000–2024 and 2081–2100.

### 2.5. High Resolution Remote Sensing Data

We used the UAV (Unmanned Aerial Vehicle) DJI Mavic 3 Multispectral to obtain very-high resolution scenes during the fieldworks conducted in July 2025. The CMOS RGB + G/R/RE/NIR cameras are installed on this UAV. The scenes were taken at an altitude of about 80 m above the ground surface with about 50% overlap. In total 1300 scenes were obtained. We preprocessed the UAV data using the Agisoft Metashape software [35].

We also analyzed hi-resolution data obtained from freely available web-services [36] with a resolution of 2.0–3.7 m for 2006 and 2024 (QuickBird, WorldView-3, Pleiades Neo) to estimate vegetation cover dynamics. Changes in the vegetation cover were determined using ESRI ArcGIS software based on the expert interpretation and semi-automatic classification procedures.

### 2.6. Dendrochronology Analysis

The total sample size included cores from 77 and 17 larch and poplar trees, respectively. Tree ring widths were measured with the precision of 0.01 mm. Missing rings were detected by the cross-dating method. The quality of cross-dating was checked by the COFECHA 6.02 software [37,38]. Age trends were eliminated by negative exponential or negative linear regression methods (using the ARSTAN 6.02 software [39,40]). Standard and residual tree ring chronologies were generated. Standard chronologies are biweight robust mean values of indexed raw chronologies. Residual chronologies were generated from standard chronologies by eliminating the autoregressive component (using AR modeling). Tree-ring chronologies (in mm) are a proxy of the annual radial increment. We used a unitless growth index (GI) as the metric of tree growth increment. GI is a normalized tree-ring chronology with an average of 1.0 and relatively constant dispersion. We used the residual chronologies in the dendroclimatic analysis [41].

### 2.7. Vegetation Productivity Data

The gross primary productivity (GPP) of vegetation cover was estimated using the MODIS MOD17A3HGF product (2001–2025) [42]. These data represent raster composites of the annual GPP values ( $\text{kgC/m}^2$ ) with a spatial resolution of 500 meters [43]. Time series data were obtained from the EarthData geoportal [44]. The original GPP data were converted into multi-band images. The average values were determined for specific areas within the 250-meter buffered zones around the test sites using the exactextract algorithm [45]. This algorithm is implemented as a Python library for extracting and summarizing the values in portions of a raster dataset [46].

The GPP trends were calculated for each pixel based on the Theil-Sen algorithm using the pyMannKendall library (v.1.4.2) [47]. It is a non-parametric method based on the Mann-Kendall Test used to analyze time series data for consistently increasing or decreasing trends [48]. Spatial changes in the GPP values between 2022–2024 and 2001–2003 were estimated using Mann-Whitney U-test implemented in the SciPy Python library [49].

### 2.8. Statistical Analysis

We used StatSoft Statistica v.10 [50], R 4.5.1 [51] along with RStudio v.2025 [52], and Microsoft Excel for statistical analysis. The geospatial analysis was performed using ESRI ArcGIS software and Python. The GPP trends were calculated based on the Theil-Sen algorithm [48] using Python. The changes in GPP were estimated using the Mann-Whitney U-test. Trends in the total water content (EWTA) and the growth index were assessed based on simple linear regression using standard methods. The difference between forecasted and historical climate was estimated using the t-test.

## 3. Results

### 3.1. Eco-Climate Variables Dynamics

Long-term improvement of the moisture regime (precipitation increase together with the decrease in air and soil droughts since the 1950s) shifted to the worsening of moisture supply since c. 1990 (Figure 3 a-c). Gravimetric measurements of the total water content indicated its long-term decrease in the 21st century (Figure 3e). However, the moisture regime improved during the last decade (Figure 3 a-c, e). Both summer and annual air temperature have been increasing since c. 1990 (Figure 3d).

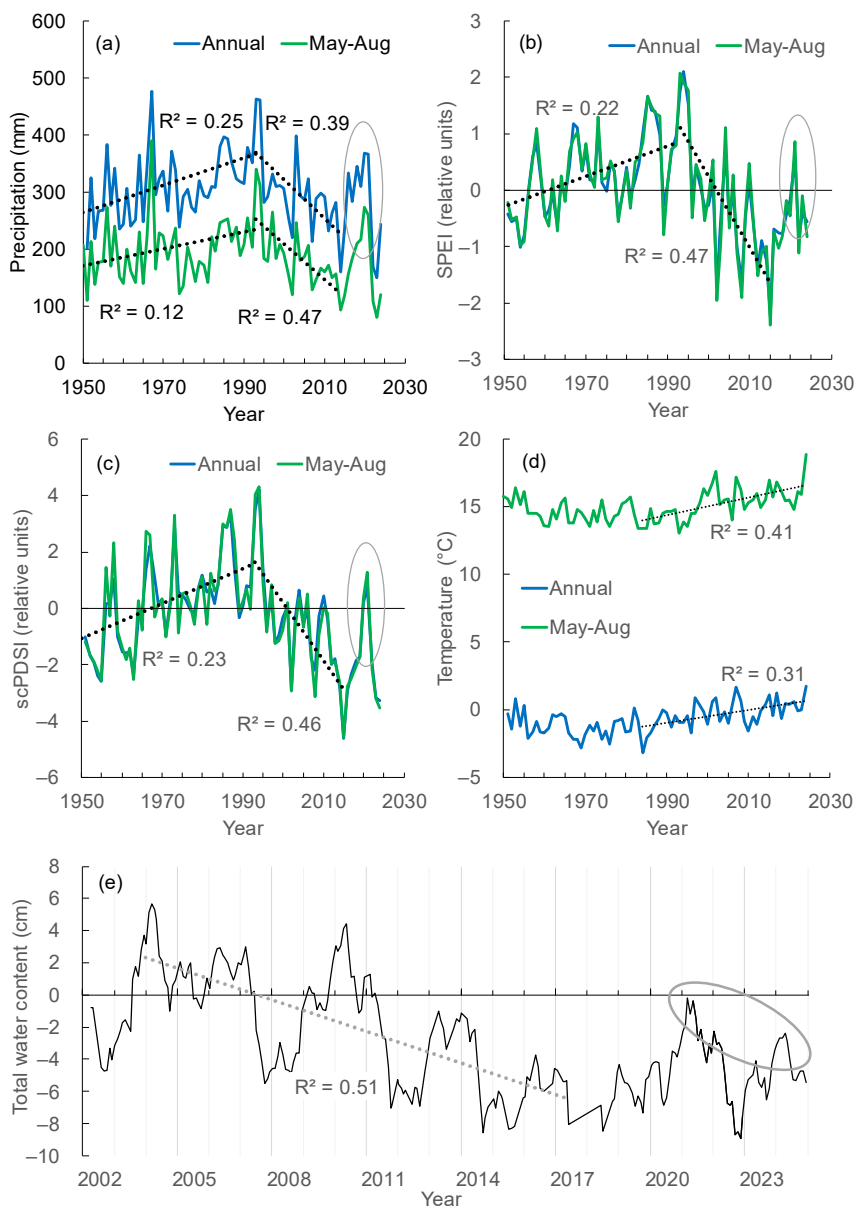


**Figure 3.** The decrease of air (SPEI) and soil (scPDSI) droughts which occurred since 1950s shifted to an increase in drought since c. 1990 (b, c). The total water content decreased since the beginning of the 21s century (e). The restart of moisture increase has been observed since 2015 (indicated by ovals on charts a–c and e). Note: decreases in SPEI and scPDSI values indicate drought increase. Air temperatures have been rising since c. 1990. Trends are significant at  $p < 0.05$ .

The wind speed, an essential variable that influences tree vigor, reached  $3.2 \text{ m s}^{-1}$  during winter with about  $0.6 \pm 0.1 \text{ m s}^{-1}$  during the growing period (May–September). The prevailing winds blow from the west and northwest (Figure 4).

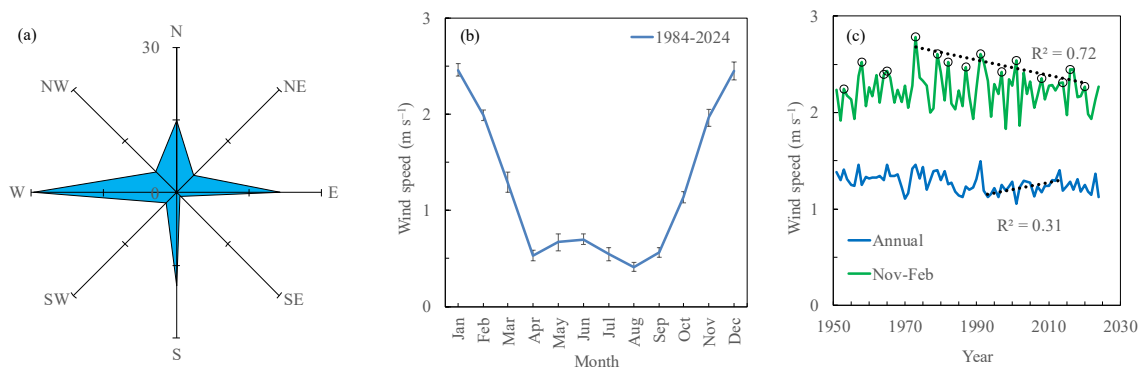


**Figure 4.** (a) Prevailing winds blow from the west and northwest directions. (b) The maximum of wind speed (up to  $3.2 \text{ m s}^{-1}$ ) occurred in December, whereas during May-September the speed falls to  $0.6 \pm 0.1 \text{ m s}^{-1}$ . (c) The maximum wind speed decreased from to  $2.8 \text{ m s}^{-1}$  (1975 y) to  $2.3 \text{ m s}^{-1}$  in 2024.

### 3.2. The Chronology of Tree Growth Index

Growth chronologies of *L. sibirica* for Tes-Hem and Kara-Haya sites were merged because both chronologies were strongly correlated ( $r = 0.68$ ) (Figure 5a).

The larch population consists of two cohorts: old-growth trees (age up to 500+y) and young generation (age up to 60 y). The formation of the young cohort corresponded to the period of air and soil drought decrease in 1980s (Figure 3 b,c; Figure 5c).

Larch growth chronologies indicated warming in the 16th century followed by the Little Ice Age in the 17th and subsequent periods of warming and cooling (Figure 5a). An interesting phenomenon observed in the year 1710, namely a sharp decrease in larch growth. The only plausible explanation for this is damage to the trees caused by a lightning strike.

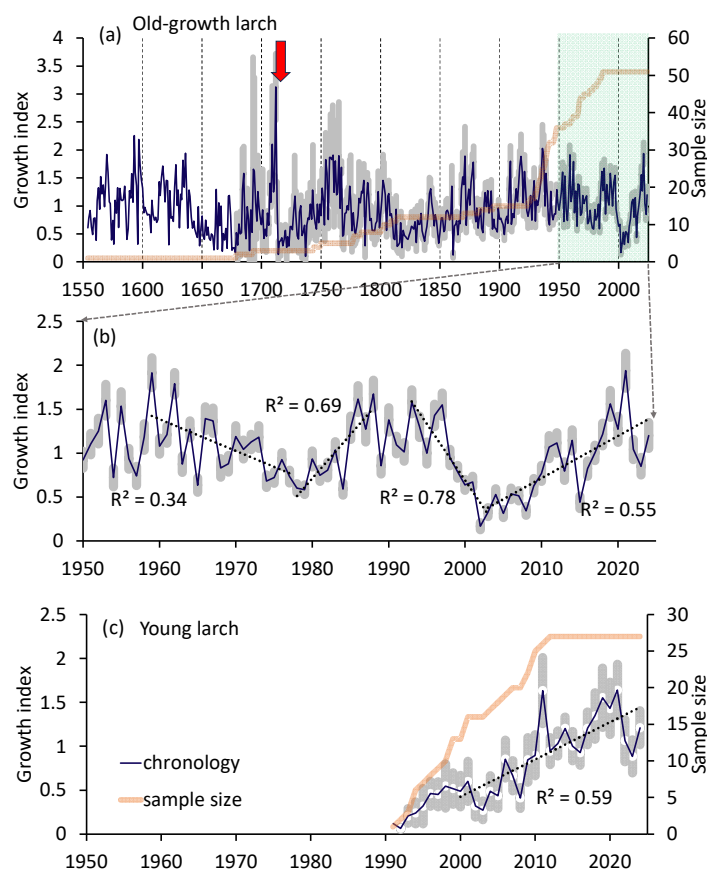


**Figure 5.** (a) Old-growth larch GI chronology. Strong GI decrease in 1713 was probably caused by a lightning strike (indicated by an arrow). (b) Old-growth larch chronology since the 1950s (marked by the green rectangle on (a)). (c) Young larch cohort chronology. Trends are significant at  $p < 0.05$ .

An air and soil drought decrease in 1980-s –1995-s stimulated larch growth with a following depression until c. 2003, followed by GI increase during the last decades (Figure 5b). The growth of the young larches was similar to that of old-growth trees (Figure 5c).

The poplar tree chronology is more stochastic in comparison with the larch chronology. Similar to larch, poplar growth decreased in 1990s and then increased in the 21st century (Figure 6).

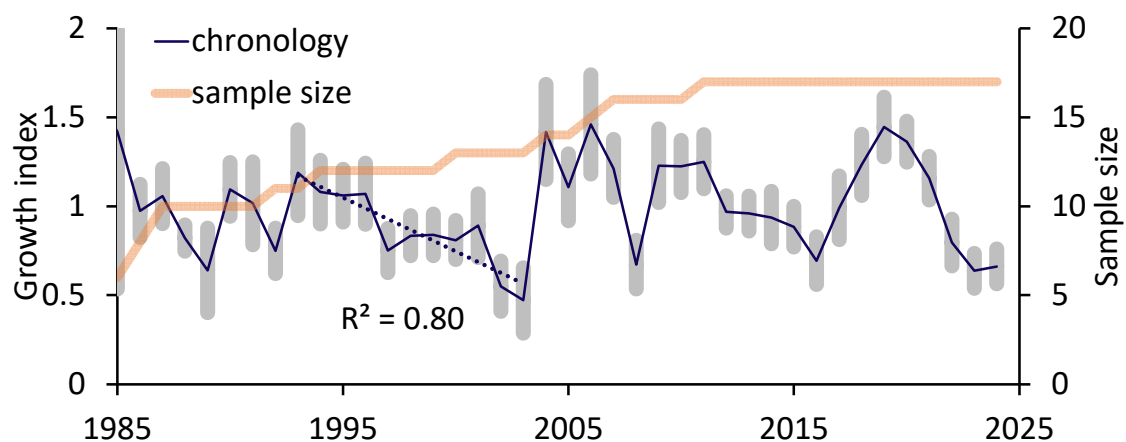


**Figure 6.** Poplar growth chronology is more stochastic in comparison with the larch chronology. After a similar growth decrease in 1990s, an increase of mean growth index values was observed after c. 2005.

### 3.3. Trees Growth Dependence on Climate Variables

Growth of both old-growth and young larch tree cohorts is controlled by the moisture variables – precipitation, air and soil droughts. Notably, there is a higher dependence of the young larch cohort in comparison with old-growth trees ( $r = 0.45...0.75$  versus  $0.30...0.49$ ) (Figure 7 b-d). This is explained by the differences in the roots habitat zone which is evidently deeper in the case of old-growth trees. Air temperature impairs young larch growth whereas its influence on the old-growth trees was insignificant (Figure 7a).

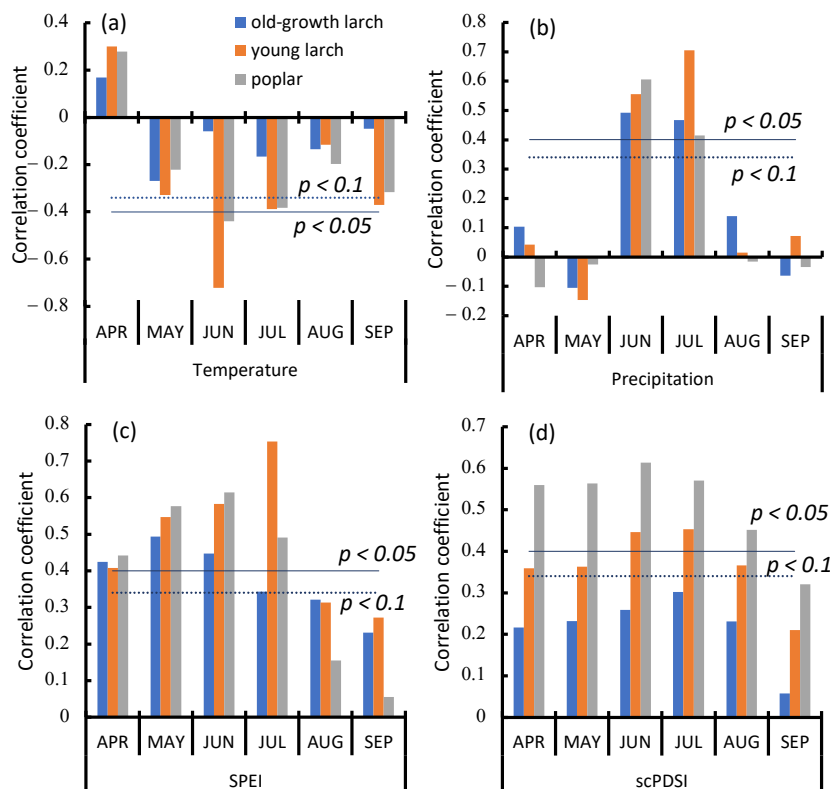


**Figure 7.** June-July temperatures impair young larch and poplar growth (a), whereas June-July precipitation stimulates larch and poplar growth (b). Air (c) and soil (d) droughts impair both species throughout the entire growth period. Old-growth larch less sensitive to the influence of climate variables. Period: 2000 – 2024. Note: decreases in SPEI and scPDSI values indicate drought increase.

Poplar trees dependence on air temperature and moisture variables is similar or stronger (in the case of soil drought) in comparison with young larch trees (Figure 7).

Summer wind (July) impaired larch growth presumably by wind-caused water loss via increasing evapotranspiration (Figure 8).

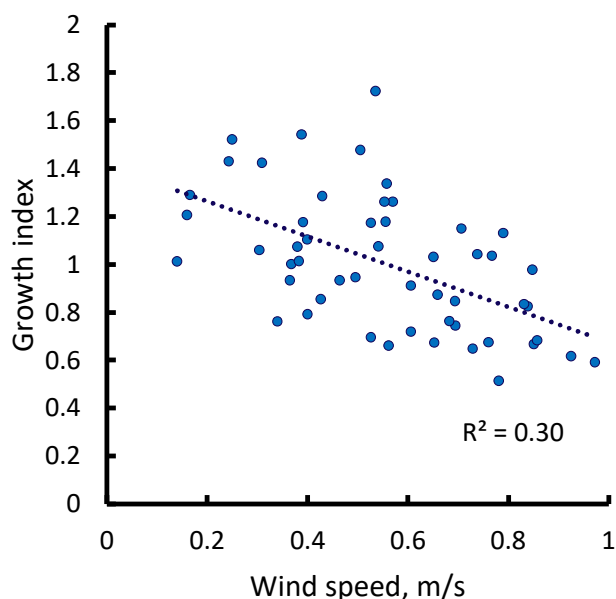


**Figure 8.** Growth index of larch trees impaired by summer (July) winds. Period: 1970–2024.

### 3.4. Trees Proagation into Desert

Surprisingly, the lesser drought-resistance poplar trees migrated into the desert further than larch trees. The average shifts of poplars and larch boundary into desert were  $35\pm 5$  m (max = 70 m) and  $280\pm 10$  m (max = 470 m) since 1985 to 2024. The year 1985 is the proxy of the larch and poplar young cohort trees establishment (Figure 9).

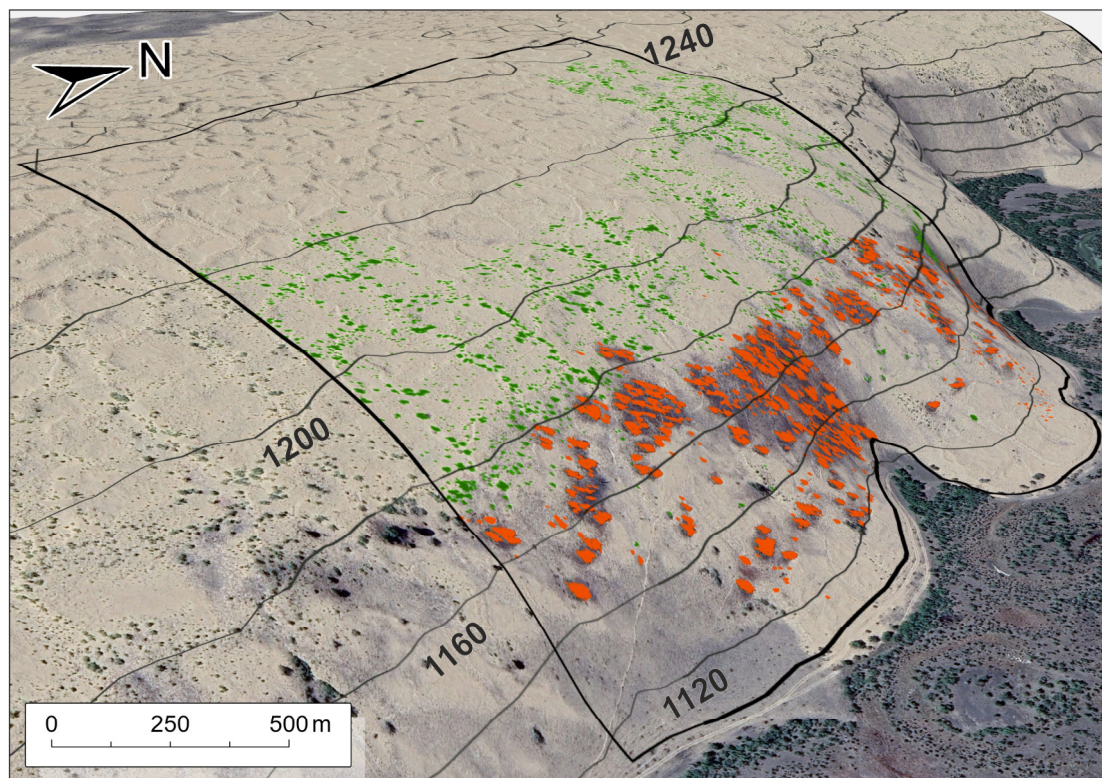


**Figure 9.** Distribution of trees on the Tes-Hem site (2024 y). Larch trees are marked in red, poplar ones in green. Trees in the refugia are protected from prevailing winds by the dune's slope.

The mean migration speed of larch and poplar were 0.9 m/y and 7.0 m/y

### 3.5. GPP Trends

Positive GPP trends cover about 76% of the sandy dunes area. The rate of GPP increase was  $\sim 19$  kg/ha/y. Mean GPP in the last five years (2020-2024) increased by 250 kgC/ha in comparison with 2002–2006 (i.e., at the beginning of observations). Currently, mean vegetation GPP is 2080 kgC/ha with max values around 6000 kgC/ha (Figure 10).

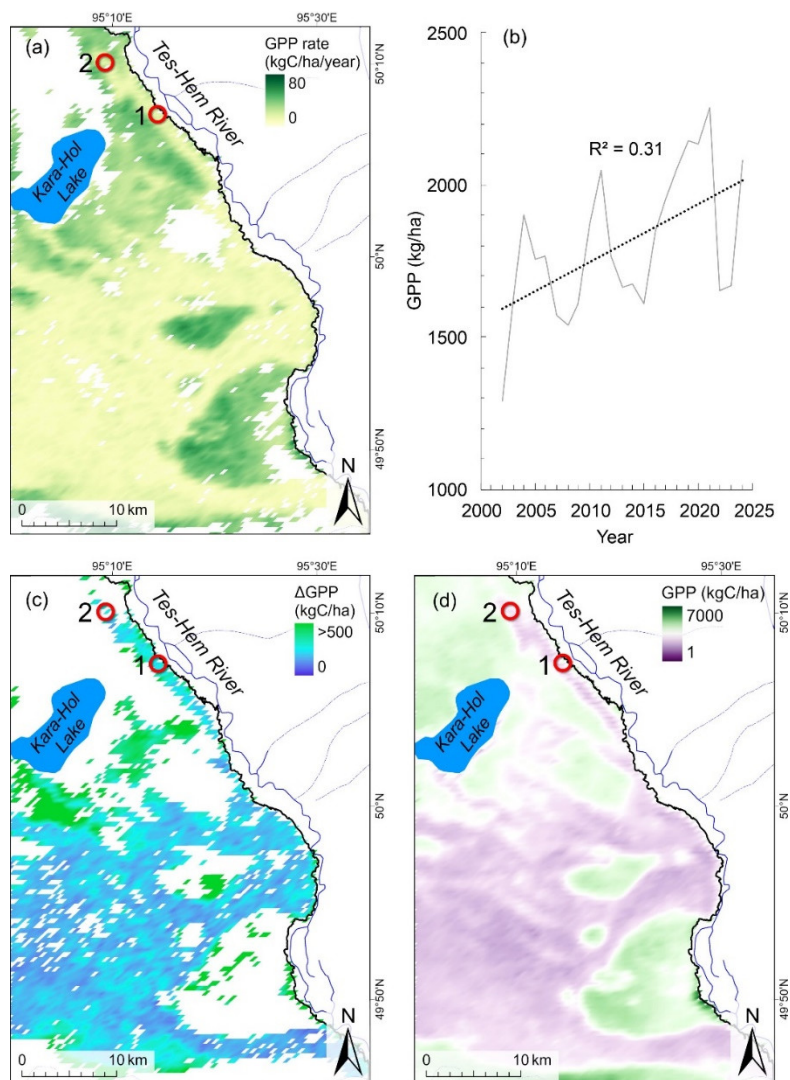


**Figure 10.** (a) Positive GPP trends cover about 76% of study area ( $S = 140,700$  ha) ( $p < 0.05$ ). (b) Mean GPP trends were increasing. The GPP rate was  $\sim 19$  kg/ha/y ( $p < 0.01$ ). (c) The mean  $\Delta$ GPP increase was 250 kgC/ha ( $\Delta$ GPP: 2020–2024 vs 2002–2006). (d) The GPP map for 2024 y. Mean GPP is 2080 kgC/ha. Study period: 2002–2024.

### 3.6. The Moisture Deficit Projections

The moisture deficit (MD) is an important hydrological parameter that indicates the moisture regime of vegetation. MD was calculated as the difference ( $\Delta$ ) between precipitation and potential evapotranspiration (PET). We estimated MD up to the end of the 21st century (2081–2100) for the climate scenarios SSP2-4.5, SSP3-7.0, and SSP5-8.5. The scenario SSP1-2.5 was not considered since it is not realistic now.

The increase of MD is predicted in the beginning and middle of the growth period (May–July) according to all climate scenarios. However, changes in the annual MD are insignificant (Figure 11).

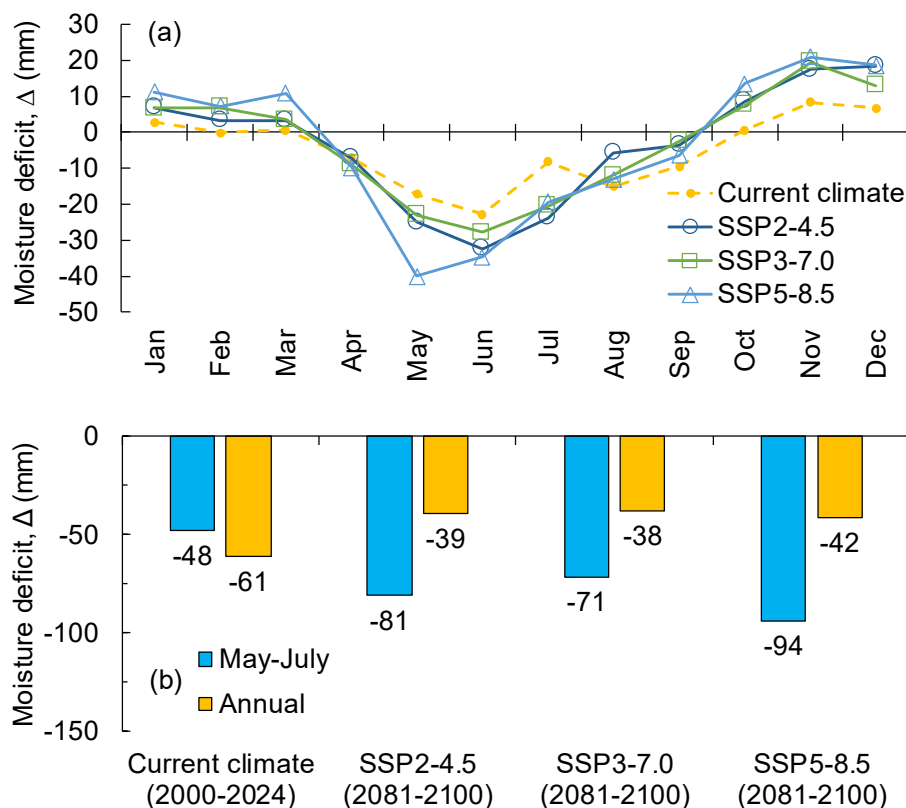


**Figure 11.** (a) Monthly and (b) annual and May-July moisture deficit (MD) in the current (2000–2024) and future (2081–2100) climates (SSP2-4.5, SSP3-7.0, and SSP5-8.5). Moisture deficit (MD) in May-July in the current climate differs from the projected MD ( $p < 0.05$ ) for all climate scenarios. The changes in the annual MD are insignificant.

#### 4. Discussion

For forest ecologists, the most significant changes in tree growth, vigor and range expected to be within the forest - non forest ecotones. In this work we considered the larch growth within unique ecotone in which larch refugia are in contact with Mongolian desert or, in broader view, with the northern boundary of the Great Goby desert. The age of alive larch in refugia exceeds 500 years which suggests that this “last larch frontier” has existed throughout the Holocene. Refugia is located at the edge of larch range along the geographical meridian. Trees survival in refugia is facilitated by site relief features. Namely, trees grow on sheltered downwind north-west and south-west slopes and within local depressions. These are the zones of the snow accumulation and lower evapotranspiration.

Larch population in the refugia includes old-growth and young tree cohorts (age  $A = 50+$ ). Young cohort establishment corresponds to the end of 1970th, when warming coincided with local minimum of air and soil drought (Figure 3 a-d). Then, when warming-driven water stress increased in 1990s, both tree growth and regeneration recruitment decreased, followed by an increase in the 21st century (Figure 5). In the 21-s century, the population of *L. sibirica* increased by +36%.

Larch growth response to a warming climate included several phases. First, since warming began in the 1970s, growth increased. Then, growth stagnation and decrease were observed in the late 1990s and very beginning of the 2000s, associated increased water stress. Finally, in the 21st century larch growth rose against the background of decreasing air and soil drought (Figure 5).

Indeed, larch growth is strongly controlled by the moisture variables – air (SPEI index) and soil (Palmer’s scPDSI index) droughts (Figure 7c, d). Old-growth larch is less sensitive to moisture stress than young larch, which is evidently explained by its deeper root habitat. Young trees are also more sensitive to the negative influence of temperature at the beginning of the growing period (Figure 7a).

This influence is mostly indirect, i.e., caused by increased water loss. However, warming has stimulated larch growth in the southern Siberian and northern China mountains [5,9].

It is notable that summer winds impaired larch growth, whereas the influence of winter wind was insignificant (Figure 8). This influence explained by increased water loss through evapotranspiration. Typically, winter winds impair trees growth due to desiccation and snow abrasion [53]. However, in the study area winter wind speed is low (~3.0 m/s) and its maximal values are decreasing (Figure 4b, c). In addition, larches are protected by the dune's slope against prevailing winds (Figure 9).

Similarly to larch, relict Scots pine (*Pinus sylvestris* L.) at its southern edge is also showing increasing growth and regeneration density in the 21st century (Figure 12a) [54,55]. This pine refugia is located northward in the Tuva hollow. Both species are growing on the sandy dunes. Pine is also a drought-resistant species, although its resistance to moisture stress is lower (Figure 12 b, c). Therefore, the pine southern boundary is located at c. 100 km northward. Unlike larch, relict pines have experienced an increasing wild fire influence that has damaged mature trees and, more importantly, burned regeneration. So, the existence of this unique refugia depends on the combination of available moisture and burning rate.

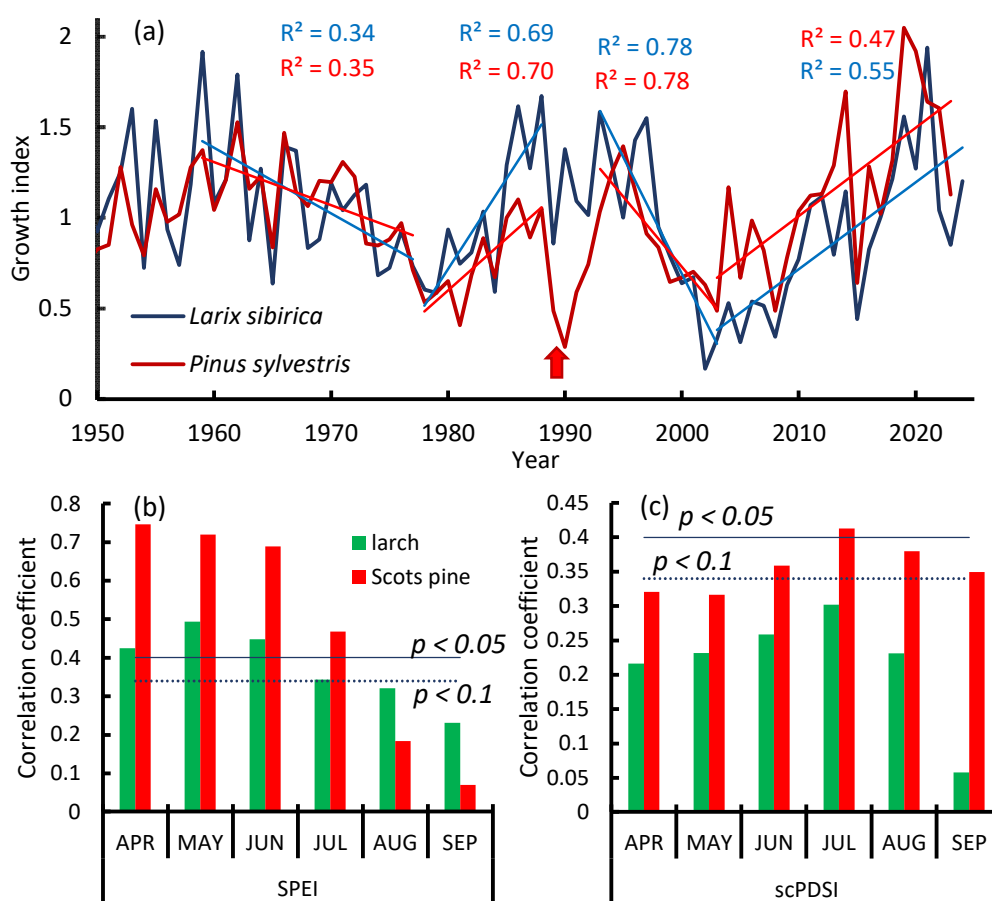


**Figure 12.** (a) *L. sibirica* and *P. sylvestris* chronologies are synchronized ( $r = 0.66$ ). An arrow indicates a severe wildfire in the pine refugia (b) Scots pine is more sensitive to air (SPEI) and (c) soil droughts (scPDSI). Horizontal lines indicate the level of significance.

Opposite to reported shrinkage of larch range at its southern edge (e.g., in the Trans-Baikal zone and in the West Sayan Mountains, [2,5]), on the boundary with the Mongolian desert larch is expanding its range. However, the above-mentioned range shrinkage is caused by an increased fire rate, whereas the desert is a no-fire area. Meanwhile, larch forest dieback has been described in the Mongolian Mountains [56]. Earlier studies also revealed larch and Scots pine growth decrease in the

Asian arid zone in the beginning of the 21st century [57,58]. However, our longer chronology indicated that both species increased growth during last two decades (Figure 12a).

Within the larch refugium a single old-growth poplar trees ( $A > 200$  y) were found (Figure 2c). The young poplar trees ( $A = 40+$  y) are located southward of the refugia (Figure 9). Similar to young larch trees, they started to establish since warming began in the 1970s. Growth of poplar trees is more strongly controlled by air and soil droughts in comparison with larch trees (Figure 7 c, d). In the 21st century, the population of *P. laurifolia* increased by +46%.

Both drought-resistant larch and less resistant poplar were slowly migrating into the adjacent desert. Unexpectedly, poplar trees migrated ahead of larch (mean shift and speed are 280 m and 7 m/y vs 35 m and 0.9 m/y for larch). The mean speed of the larch trees migration was about 0.9 m/y, which is about twice as high as the rate of larch and other conifer migration into alpine tundra [53]. Poplar migration speed is about one order higher (7 m/y). *Populus* propagation facilitated by its high seed productivity ( $> 1$  million seeds for a mature tree). Light seeds with “parachutes” spread over hundreds of meters. In addition, individuals can also reproduce through the roots by suckers. Because of that, poplar regeneration reached 900 seedlings/ha, whereas larch regeneration is sporadic. Therefore, the new niches created by the changing moisture regime are colonized by *P. laurifolia* ahead of larch.

Trees growth increase coincided with GPP increase of vegetation (composed by small bushes) in adjacent sands. That represents a “greening” of the Gobi Desert at its northern boundary. Similar phenomenon has been observed in the nearby Tuva hollow, where steppe communities are increasing their GPP [54,55]. It is worth noting that described increase in population of trees and shrubs has facilitated sands conservation and suppressed desert northward migration.

In general, we observed a unique event of southward migration of trees at the edge of their range, whereas in number of publications describe tree species range shrinkage at their southern boundary (e.g., [11,59]). For example, *P. tremuloides* Michx. has experienced negative climate-driven changes in the North American forests [60]. *Larix gmelinii* decline and mortality have been described in the Trans-Baikal zone [12,61], *Betula* sp. in Mongolia and the Trans-Baikal zone [62,63]. Conifer mortality at their southern range has been described in Europe and America [64–66]. However, predicted increase of moisture deficit and worsening of the hydrological regime (with horizon to 2080–2100) suggests a decrease of trees ranges in the studied zone. Nevertheless, the changing climate is currently favorable for the growth of trees and bushes at the northern boundary of the Great Gobi Desert.

## 5. Conclusions

At the southern edge of larch and poplar ranges we observed a unique southward migration of trees, while published studies revealed the shrinkage of tree species at their southern ranges throughout the boreal biome. Moreover, trees are migrating from refugia into sandy dunes. Notably, *P. laurifolia* migration rate is about one order of magnitude faster than that of *L. sibirica*. Alongside that, GPP of vegetation cover in the desert is increasing. Currently, climate warming is favorable for the growth of trees and bushes at the northern boundary of the Great Gobi Desert.

**Author Contributions:** conceptualization, V.I.K., I.A.P.; methodology, V.I.K., I.A.P., S.T.I, A.S.S.; validation, V.I.K., I.A.P., S.T.I, A.S.S.; formal analysis, I.A.P., A.S.S., S.T.I.; investigation, V.I.K., I.A.P.; S.T.I., A.S.S.; resources, A.S.S., S.T.I., S.O.O.; data curation, I.A.P., A.S.S., S.T.I., A.M.S.; writing—original draft preparation, V.I.K., I.A.P., S.T.I.; visualization, I.A.P., A.S.S., S.T.I.; supervision, V.I.K. I.A.P.; project administration, V.I.K.; funding acquisition, V.I.K. Authors have read and agreed to the published version of the manuscript.

**Funding:** The research was funded by the Basic Project of the Federal Research Center of the Scientific Center, no. FWES-2024-0023.

**Data Availability Statement:** The data presented in this study are openly available: climate data at <https://cds.climate.copernicus.eu/cdsapp> (accessed on 21 January 2026) and from the AISORI web-service (<http://aisori-m.meteo.ru/waisori/>; accessed on 21 January 2026); GPP data at <https://lpdaac.usgs.gov/products/mod17a2hv006/>; EWTA data at NASA GRACE(-FO) (accessed on 21 January 2026) Data Analysis Tool (<https://grace.jpl.nasa.gov/data/data-analysis-tool/>; accessed on 21 January 2026); CMIP6 data at IPCC WGI Interactive Atlas service (<https://interactive-atlas.ipcc.ch/>; accessed on 21 January 2026).

**Conflicts of Interest:** The authors declare no conflict of interest.

## Abbreviations

The following abbreviations are used in this manuscript:

UAV	Unmanned Aerial Vehicles
GI	Growth Index
GPP	Gross Primary Production
PET	Potential Evapotranspiration
MD	Moisture Deficit
SSP	Shared Socioeconomic Pathway
scPDSI	Self-Calibrated Palmer Drought Severity Index
SPEI	Standardized Precipitation Evapotranspiration Index
DBH	Diameter at Breast Height
WMO	World Meteorological Organization
TWC	Total Water Content
GRACE	Gravity Recovery And Climate Experiment
EWTA	Equivalent Water Thickness Anomalies
PRE	Precipitation
E	Evaporation
TS	Test Sites

## References

1. Kloeppel, B.; Gower, S.; Treichel, I.; et al. Foliar carbon isotope discrimination in *Larix* species and sympatric evergreen conifers: a global comparison. *Oecologia* **1998**, *114*, 153–159. <https://doi.org/10.1007/s004420050431>.
2. Kharuk, V.I.; Shvetsov, E.G.; Buryak, L.V.; Golyukov, A.S.; Dvinskaya, M.L.; Petrov, I.A. Wildfires in the Larch Range within Permafrost, Siberia. *Fire* **2023**, *6*, 301. <https://doi.org/10.3390/fire6080301>.
3. Kharuk, V.I.; Im, S.T.; Petrov, I.A.; Dvinskaya, M.L.; Shushpanov, A.S.; Golyukov, A.S. Climate-Driven Conifer Mortality in Siberia. *Global Ecology and Biogeography* **2021**, *30*(2), 543–556. <https://doi.org/10.1111/geb.13243>.
4. Shiyatov, S.G.; Terent'ev, M.M.; Fomin, V.V.; et al. Altitudinal and horizontal shifts of the upper boundaries of open and closed forests in the Polar Urals in the 20th century. *Russ. J. Ecol.* **2007**, *38*, 223–227. <https://doi.org/10.1134/S1067413607040017>.
5. Kharuk, V.I.; Petrov, I.A.; Golyukov, A.S.; et al. Larch growth across thermal and moisture gradients in the Siberian Mountains. *J. Mt. Sci.* **2023**, *20*, 101–114. <https://doi.org/10.1007/s11629-022-7433-3>.
6. Kirdeyanov, A.V.; Prokushkin, A.S.; Tabakova, M.A. Tree-ring growth of Gmelin larch under contrasting local conditions in the north of Central Siberia. *Dendrochronologia* **2013**, *31*, 114–119. <https://doi.org/10.1016/j.dendro.2012.10.003>.
7. Kharuk, V.I.; Ranson, K.J.; Petrov, I.A.; Dvinskaya, M.L.; Im, S.T.; Golyukov, A.S. Larch (*Larix dahurica* Turcz) growth response to climate change in the Siberian Permafrost Zone. *Reg. Environ. Change* **2018**. <https://doi.org/10.1007/s10113-018-1401-z>.
8. Grigoriev, A.A.; Shalaumova, Y.V.; Vyukhin, S.O.; Balakin, D.S.; Kukarskikh, V.V.; Vyukhina, A.A.; Camarero, J.J.; Moiseev, P.A. Upward Treeline Shifts in Two Regions of Subarctic Russia Are Governed by Summer Thermal and Winter Snow Conditions. *Forests* **2022**, *13*, 174. <https://doi.org/10.3390/f13020174>.

9. Zhang, X.; Ba, X.; Chang, Y.; Chen, Z. Increased sensitivity of Dahurian larch radial growth to summer temperature with the rapid warming in Northeast China. *Trees* **2016**, *30*, 1799–1806. <https://doi.org/10.1007/s00468-016-1413-6>.
10. Kharuk, V.I.; Petrov, I.A.; Dvinskaya, M.L.; et al. Comparative reaction of larch (*Larix sibirica* Ledeb) radial increment to climate change in the forest-steppe and highlands of Southern Siberia. *Contemp. Probl. Ecol.* **2018**, *11*(4), 388–395. <https://doi.org/10.1134/S1995425518040042>.
11. Anderegg, W.R.L.; Wu, C.; Acil, N.; Carvalhais, N.; Pugh, T.A.M.; Sadler, J.P.; Seidl, R. A climate risk analysis of Earth's forests in the 21st century. *Science* **2022**, *377*, 1099–1103. <https://doi.org/10.1126/science.abp9723>.
12. Mamet, S.D.; Brown, C.D.; Trant, A.J.; Laroque, C.P. Shifting global *Larix* distributions: Northern expansion and southern retraction as species respond to changing climate. *J. Biogeogr.* **2019**, *46*(1), 30–44.
13. Specialized arrays for climate research. All-Russia Research Institute of Hydrometeorological Information – World Data Center. Available online: <http://aisori-m.meteo.ru/waisori/index.xhtml?idata=2> (accessed on 21 January 2026). (In Russian)
14. Liu, Q.; Yang, S.; Li, S.; Zhang, H.; Zhang, J.; Fan, H. The optimal applications of scPDSI and SPEI in characterizing meteorological drought, agricultural drought and terrestrial water availability on a global scale. *Sci. Total Environ.* **2024**, *952*, 175933.
15. Wells, N.; Goddard, S.; Hayes, M.J. A self-calibrating Palmer Drought Severity Index. *J. Clim.* **2004**, *17*, 2335–2351.
16. Beguería, S.; Vicente-Serrano, S.M. SPEI: Calculation of the Standardized Precipitation-Evapotranspiration Index. 2023. Available online: <https://spei.csic.es>, <https://github.com/sbegueria/SPEI> (accessed on 21 January 2026).
17. Beguería, S.; Vicente-Serrano, S.M. *SPEI*: [R package]. Available online: <https://cran.r-project.org/web/packages/SPEI> (accessed on 21 January 2026).
18. *RStudio Desktop*: [Software]. Available online: <https://posit.co/download/rstudio-desktop> (accessed on 21 January 2026).
19. CRAN (RStudio mirror): [Repository]. Available online: <https://cran.rstudio.com/> (accessed on 21 January 2026).
20. *scPDSI*: [Software repository]. Available online: <https://github.com/Sibada/scPDSI> (accessed on 21 January 2026).
21. Muñoz Sabater, J. ERA5-Land monthly averaged data from 1950 to present. Copernicus Climate Change Service (C3S) Climate Data Store (CDS), 2019. Available online: <https://cds.climate.copernicus.eu/datasets/reanalysis-era5-land-monthly-means?tab=overview> (accessed on 21 January 2026).
22. *GRACE Data Analysis Tool*: [Online data service]. Available online: <https://grace.jpl.nasa.gov/data/data-analysis-tool/> (accessed on 21 January 2026).
23. Landerer, F.W.; Swenson, S.C. Accuracy of scaled GRACE terrestrial water storage estimates. *Water Resour. Res.* **2012**, *48*, W04531. <https://doi.org/10.1029/2011WR011453>.
24. Wahr, J.; Molenaar, M.; Bryan, F. Time-variability of the Earth's gravity field: Hydrological and oceanic effects and their possible detection using GRACE. *J. Geophys. Res.* **1998**, *103*(B12), 30205–30229. <https://doi.org/10.1029/98JB02844>.
25. Middendorf, K.; Dobsław, H.; Jensen, L.; Eicker, A. Return levels of dry extreme events in terrestrial water storage from satellite gravimetry and CMIP6 global coupled climate models. *J. Geophys. Res. Solid Earth* **2025**, *130*(10), e2024JB031011. <https://doi.org/10.1029/2024JB031011>.
26. Cheng, Y.; An, Q.; Liu, L.; Li, H.; Huang, G. Spatially distinct drought patterns and influencing factors across China: A machine learning approach with a comprehensive index. *Ecol. Indic.* **2025**, *179*, 114170. <https://doi.org/10.1016/j.ecolind.2025.114170>.
27. Barbosa, S.A.; Jones, N.L.; Williams, G.P.; Teklu, H.; Yidana, S.M.; Pulla, S.T.; Sanchez, J.L.; Nelson, E.J.; Ames, D.P.; Miller, A.W. A multi-source approach to groundwater storage and recharge assessment in the Volta Basin. *Sci. Total Environ.* **2025**, *1001*, 180421. <https://doi.org/10.1016/j.scitotenv.2025.180421>.

28. Wang, Z.; Bi, Y.; Yang, F.; Zheng, J.; Yang, Y.; Zhang, S. Research of spatial-temporal variation and correlation of water storage and vegetation coverage in the Loess Plateau. *Remote Sens.* **2025**, *17*(17), 2983. <https://doi.org/10.3390/rs17172983>.
29. Kharuk, V.I.; Im, S.T.; Dvinskaya, M.L.; Golyukov, A.S.; Ranson, K.J. Climate-induced mortality of spruce stands in Belarus. *Environ. Res. Lett.* **2015**, *10*(12), 125006. <https://doi.org/10.1088/1748-9326/10/12/125006>.
30. Kharuk, V.I.; Im, S.T.; Petrov, I.A.; Shvetsov, E.G. Permafrost Degradation and Vegetation Growth Beyond the Polar Circle in Siberia. *Forests* **2025**, *16*(1), 47. <https://doi.org/10.3390/f16010047>.
31. Voldoire, A.; Saint-Martin, D.; Sénési, S.; Decharme, B.; Alias, A.; Chevallier, M.; Colin, J.; Guérémy, J.-F.; Michou, M.; Moine, M.-P.; Nabat, P.; Roehrig, R.; Salas y Mélia, D.; Séférian, R.; Valcke, S.; Beau, I.; Belamari, S.; Berthet, S.; Cassou, C.; Cattiaux, J.; Deshayes, J.; Douville, H.; Ethé, C.; Franchistéguy, L.; Geoffroy, O.; Lévy, C.; Madec, G.; Meurdesoif, Y.; Msadek, R.; Ribes, A.; Sanchez-Gomez, E.; Terray, L.; Waldman, R. Evaluation of CMIP6 DECK experiments with CNRM-CM6-1. *J. Adv. Model. Earth Syst.* **2019**, *11*(7), 2177–2213. <https://doi.org/10.1029/2019MS001683>.
32. IPCC Interactive Atlas: [Online atlas]. Available online: <https://interactive-atlas.ipcc.ch/> (accessed on 21 January 2026).
33. Gutiérrez, J.M.; Jones, R.G.; Narisma, G.T.; Alves, L.M.; Amjad, M.; Gorodetskaya, I.V.; Grose, M.; Klutse, N.A.B.; Krakovska, S.; Li, J.; Martínez-Castro, D.; Mearns, L.O.; Mernild, S.H.; Ngo-Duc, T.; van den Hurk, B.; Yoon, J.H. *Climate Change 2021: The Physical Science Basis. Contribution of Working Group I to the Sixth Assessment Report of the Intergovernmental Panel on Climate Change* (Masson-Delmotte, V.; Zhai, P.; et al., Eds.); Cambridge University Press: Cambridge, UK, and New York, NY, USA, 2021; Interactive Atlas. Available online: <https://interactive-atlas.ipcc.ch/> (accessed on 21 January 2026).
34. IPCC. *Climate Change 2023: Synthesis Report. Contribution of Working Groups I, II and III to the Sixth Assessment Report of the Intergovernmental Panel on Climate Change* (Core Writing Team; Lee, H.; Romero, J., Eds.); IPCC: Geneva, Switzerland, 2023. Available online: [https://www.ipcc.ch/report/ar6/syr/downloads/report/IPCC\\_AR6\\_SYR\\_FullVolume.pdf](https://www.ipcc.ch/report/ar6/syr/downloads/report/IPCC_AR6_SYR_FullVolume.pdf) (accessed on 21 January 2026).
35. Agisoft: [Company website]. Available online: <https://www.agisoft.com/> (accessed on 21 January 2026).
36. Google Earth: [Web-based interactive mapping service]. Available online: <https://earth.google.com/web/> (accessed on 21 January 2026).
37. Tree-Ring Laboratory Software Resources: [Web page]. Available online: <https://www.ldeo.columbia.edu/tree-ring-laboratory/resources/software> (accessed on 21 January 2026).
38. Holmes, R.L. Computer-assisted quality control in tree-ring dating and measurement. *Tree-Ring Bull.* **1983**, *44*, 69–75.
39. Tree-Ring Laboratory: Software Resources. Available online: <https://www.ldeo.columbia.edu/tree-ring-laboratory/resources/software> (accessed on 21 January 2026).
40. Cook, E.R.; Holmes, R.L. *Chronology Development, Statistical Analysis. Guide for Computer Program ARSTAN*; Lab. of Tree Ring Res., the University of Arizona: Tucson, AZ, USA, 1986, pp. 50–65.
41. Speer, J.H. *Fundamentals of Tree-Ring Research*; University of Arizona Press: Tucson, AZ, USA, 2010.
42. Running, S.W.; Zhao, M. *User's Guide Daily GPP and Annual NPP (MOD17A2H/A3H) and Year-end Gap-Filled (MOD17A2HGF/A3HGF) Products NASA Earth Observing System MODIS Land Algorithm (For Collection 6.1)*; 2021. Available online: [https://lpdaac.usgs.gov/documents/972/MOD17\\_User\\_Guide\\_V61.pdf](https://lpdaac.usgs.gov/documents/972/MOD17_User_Guide_V61.pdf) (accessed on 21 January 2026).
43. MOD17A2H V006: [Data product]. Available online: <https://lpdaac.usgs.gov/products/mod17a2hv006> (accessed on 21 January 2026).
44. NASA Earthdata: [Data portal]. Available online: <https://www.earthdata.nasa.gov/> (accessed on 21 January 2026).
45. exactextract: [Software repository]. Available online: <https://isciences.github.io/exactextract/> (accessed on 21 January 2026).
46. exactextract [Python package]. Available online: <https://pypi.org/project/exactextract/> (accessed on 21 January 2026).

47. *pymannkendall* [Python package]. Available online: <https://pypi.org/project/pymannkendall/> (accessed on 21 January 2026).
48. Hussain, M.; Mamouei, M.; Khatibi, R. *pyMannKendall*: A Python package for non-parametric Mann-Kendall family of trend tests. *J. Open Source Softw.* **2019**, *4*(39), 1556. <https://doi.org/10.21105/joss.01556>.
49. *SciPy*: [Scientific computing software]. Available online: <https://scipy.org/> (accessed on 21 January 2026).
50. *StatSoft*: [Statistical software and solutions provider]. Available online: <http://statsoft.ru/> (accessed on 21 January 2026).
51. *R Project*: [Free software environment for statistical computing and graphics]. Available online: <https://www.r-project.org/> (accessed on 21 January 2026).
52. *Posit*: [Software and tools for data science and R/Python development]. Available online: <https://posit.co/> (accessed on 21 January 2026).
53. Kharuk, V.I.; Petrov, I.A.; Im, S.T.; Golyukov, A.S.; Dvinskaya M. L.; Shushpanov, A.S. Tree clusters migration into alpine tundra, Siberia. *J. Mountain Sci.* **2022**, *19*(12), 3426–3440. <https://doi.org/10.1007/s11629-022-7555-7>.
54. Kharuk, V.I.; Petrov, I.A.; Shushpanov, A.S.; Im, S.T.; Ondar, S.O. Scots Pine at Its Southern Range in Siberia: A Combined Drought and Fire Influence on Tree Vigor, Growth, and Regeneration. *Forests* **2025**, *16*, 819. <https://doi.org/10.3390/f16050819>
55. Petrov, I.A.; Kharuk, V.I.; Shushpanov, A.S.; et al. Erratum to: Scots Pine (*Pinus sylvestris* L.) on the Southern Border of Its Range in Siberia: Growth Dynamics under Changing Climate Conditions. *Contemp. Probl. Ecol.* **2025**, *18*, 983. <https://doi.org/10.1134/S1995425525060022>.
56. Juříčka, D.; Novotná, J.; Houška, J.; Pařílková, J.; Hladký, J.; Pecina, V.; et al. Large-scale permafrost degradation as a primary factor in *Larix sibirica* forest dieback in the Khentii massif, northern Mongolia. *J. For. Res.* **2020**, *31*(1), 197–208. <https://doi.org/10.1007/s11676-018-0866-4>.
57. Liu, H.; Williams, A.P.; Allen, C.D.; et al. Rapid warming accelerates tree growth decline in semi-arid forests of Inner Asia. *Glob. Change Biol.* **2013**, *19*, 2500–2510. <https://doi.org/10.1111/gcb.12217>.
58. Wu, X.; Liu, H.; Guo, D.; Anenkhonov, O.A.; Badmaeva, N.K.; et al. Growth decline linked to warming-induced water limitation in hemi-boreal forests. *PLoS ONE* **2012**, *7*(8), e42619. <https://doi.org/10.1371/journal.pone.0042619>.
59. Boonman, C.C.F., Serra-Diaz, J.M., Hoeks S., et al. More than 17,000 tree species are at risk from rapid global change. *Nat. Commun.* **2024**, *15*, 166. <https://doi.org/10.1038/s41467-023-44321-9>.
60. Boyd M. A., Berner L. T., Doak P., Goetz S. J., Rogers B. M., Wagner D., Walker X. J., Mack M. C. Impacts of climate and insect herbivory on productivity and physiology of trembling aspen (*Populus tremuloides*) in Alaskan boreal forests. *Environ. Res. Lett.* **2019**, *14*, 085010. <https://doi.org/10.1088/1748-9326/ab215f>.
61. Buryak, L.V.; Kalenskaya, O.P.; Kukavskaya, E.A.; Luzganov, A.G. *Zonal and geographical features of the impact of fires on forest formation of light coniferous stands in the south of Siberia*; Nauka: Novosibirsk, Russia, 2022. (In Russian)
62. Verhoeven, D.; de Boer, W.F.; Henkens, R.J.H.G.; Sass-Klaassena, U.G.W. Water availability as driver of birch mortality in Hustai National Park, Mongolia. *Dendrochronologia* **2018**, *49*, 127–133. <https://doi.org/10.1016/j.dendro.2018.04.001>.
63. Kharuk V. I., Kuzmichev V. V., Im S. T., Ranson K. J. Birch stands growth increase in Western Siberia. *Scand. J. For. Res.* **2014**, *29*(5), 421–426. <https://doi.org/10.1080/02827581.2014.912345>.
64. Martínez-Vilalta, J.; Lloret, F.; Breshears, D.D. Drought-induced forest decline: Causes, scope and implications. *Biol. Lett.* **2012**, *8*, 689–691. <https://doi.org/10.1098/rsbl.2011.1059>.
65. Millar, C.I.; Stephenson, N.L. Temperate forest health in an era of emerging megadisturbance. *Science* **2015**, *349*, 823–826. <https://doi.org/10.1126/science.aaa9933>.
66. Davis, F.W.; Parkinson, A.-M.; Moritz, M.A.; Isaac, W.; Park, C.M.; D’Antonio, C.M. Increasing vulnerability of an endemic Mediterranean-climate conifer to changing climate and fire regime. *Front. For. Glob. Change* **2025**, *8*, 1516623. <https://doi.org/10.3389/ffgc.2025.1516623>.

**Disclaimer/Publisher’s Note:** The statements, opinions and data contained in all publications are solely those of the individual author(s) and contributor(s) and not of MDPI and/or the editor(s). MDPI and/or the editor(s)

disclaim responsibility for any injury to people or property resulting from any ideas, methods, instructions or products referred to in the content.